Formation of Supernarrow Borophene Nanoribbons

Haochen Wang[#], Pengcheng Ding[#], Guang-Jie Xia[#], Xiangyun Zhao[#], Wenlong E, Miao Yu^{*}, Zhibo Ma^{*}, Yang-Gang Wang^{*}, Lai-Sheng Wang, Jun Li, and Xueming Yang^{*}

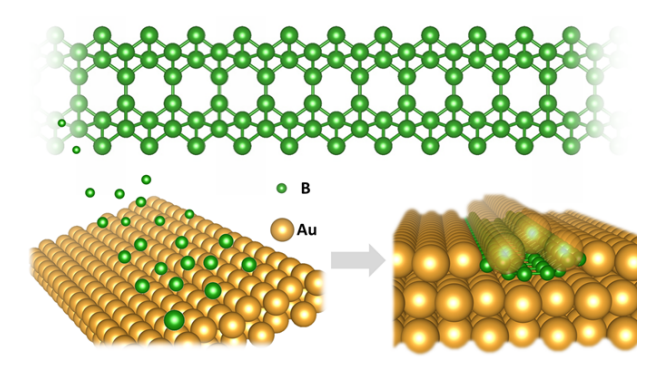
Abstract: Borophenes have sparked considerable interest owing to their fascinating physical characteristics and diverse polymorphism. However, borophene nanoribbons (BNRs) with widths less than 2 nm have not been achieved. Herein, we report the experimental realization of supernarrow BNRs. Combining scanning tunneling microscopy imaging with density functional theory modeling and ab initio molecular dynamics simulations, we demonstrate that, under the applied growth conditions, boron atoms can penetrate the outermost layer of Au(111) and form BNRs composed of a pair of zigzag (2,2) boron rows. The BNRs have a width self-contained to ~1 nm and dipoles at the edges to keep them separated. They are embedded in the outermost Au layer and shielded on top by the evacuated Au atoms, free of the need for post-passivation. Scanning tunneling spectroscopy reveals distinct edge states, primarily attributed to the localized spin at the BNRs' zigzag edges. This work adds a new member to the boron material family and introduces a new physical feature to borophenes.

Since 200 BC, boron (B) has been widely employed in glass, ceramics, medicine, machinery, fertilizer, and other industrial production. $^{[1,2]}$ As the neighbor in the periodic table, B shares certain similar properties with carbon, e.g., allowing sp^2 hybridization and electron delocalization. $^{[2,3-6]}$ B has abundant allotropes in various dimensions. $^{[2,7]}$ The most common bulk B crystal is a semiconductor made of B_{12} icosahedral units, with a hardness only slightly lower than diamond. $^{[2]}$ In analogy with graphene, B also has two-dimensional (2D) forms, *i.e.*, borophenes, $^{[8-11]}$ which are metallic and composed of triangular lattices and hollow hexagons, $^{[8,12]}$ exhibiting fascinating features,

such as in-plane anisotropy, [13–15] metallic Dirac fermions, [16,17] phonon-mediated superconductivity, great mechanical strength, and high thermal conductivity. [18–21] B polymorphism not only demonstrates the beauty of chemistry but also introduces novel physical properties. [3,4,7,21–27]

Patterning graphene into one-dimensional (1D) forms, such as graphene nanoribbons, [28-30] has been demonstrated to be an efficient strategy for introducing new intriguing electronic properties, *e.g.*, coupled spin centers and nontrivial electronic states. [31,32] According to theoretical prediction, [33,34] borophenes also have 1D forms. Encouragingly, narrow domains of 2D borophenes (with an average width of ~10 nm), striped phases of borophenes, and ribbons patterned by substrate step edges have been successfully fabricated. [27,35] Still, true 1D B allotropes with widths less than 2 nm have not been achieved. Even if they could be produced, how to properly passivate the ribbons and avoid their lateral aggregation remains a foreseeable challenge.

Herein, we report the experimental realization of 1D supernarrow borophene nanoribbons (BNRs). The BNRs are composed of a pair of (2,2) zigzag B rows (Scheme 1). Each single row's broadest and narrowest regions contain two B atoms. The BNRs have a uniform width of ~10 Å and lengths up to 200 Å. Combining scanning tunneling microscopy (STM) imaging with density functional theory (DFT) modeling and *ab initio* molecular dynamics (AIMD) simulations, we demonstrate that, under the applied growth conditions, B atoms can spontaneously penetrate the outermost layer of Au(111). They accumulate and bond with one another into BNRs, shielded on top by the evacuated Au atoms. Scanning tunneling spectroscopy (STS) reveals distinct edge states, attributed to the localized spin at the BNR's edges.



Scheme 1. Schematic illustration of supernarrow BNR on Au(111). When B atoms are deposited at a moderate rate onto an Au(111) substrate kept at RT in ultrahigh vacuum (UHV), they penetrate the outermost Au layer and form 1D BNRs (B and Au atoms are shown in green and golden, respectively). Each BNR is composed of two pairs of (2,2) zigzag B rows, forming the hollow hexagons in the middle.

[*] Dr. H. C. Wang, Dr. X. Y. Zhao, W. L. E, Prof. M. Yu, Dr. Z. B. Ma, Prof. X. M. Yang

State Key Laboratory of Molecular Reaction Dynamics, Dalian Institute of Chemical Physics, Chinese Academy of Sciences, Dalian 116023 (China)

 $\hbox{E-mail: miaoyu_che@hit.edu.cn, ma@huayang-vac.com}\\$

Dr. P. C. Ding, Prof. M. Yu

State Key Laboratory of Urban Water Resource and Environment, School of Chemistry and Chemical Engineering, Harbin Institute of Technology, Harbin 150001 (China)

Dr. G. J. Xia, Prof. Y. G. Wang, Prof. J. Li, Prof. X. M. Yang

Department of Chemistry and Guangdong Provincial Key Laboratory of Catalytic Chemistry, Southern University of Science and Technology, Shenzhen 518055 (China)

Email: wangyg@sustech.edu.cn, xmyang@dicp.ac.cn

Prof. M. Yu

School of Materials and Energy, University of Electronic Science and Technology, Chengdu 610000 (China)

Prof. L.-S. Wang

Department of Chemistry, Brown University, Providence, Rhode Island 02912 (USA)

Prof. J. Li

Theoretical Chemistry Center, Department of Chemistry, Tsinghua University, Beijing 100084 (China)

These authors contributed equally to this work.

Supporting information for this article is given *via* a link at the end of the document.

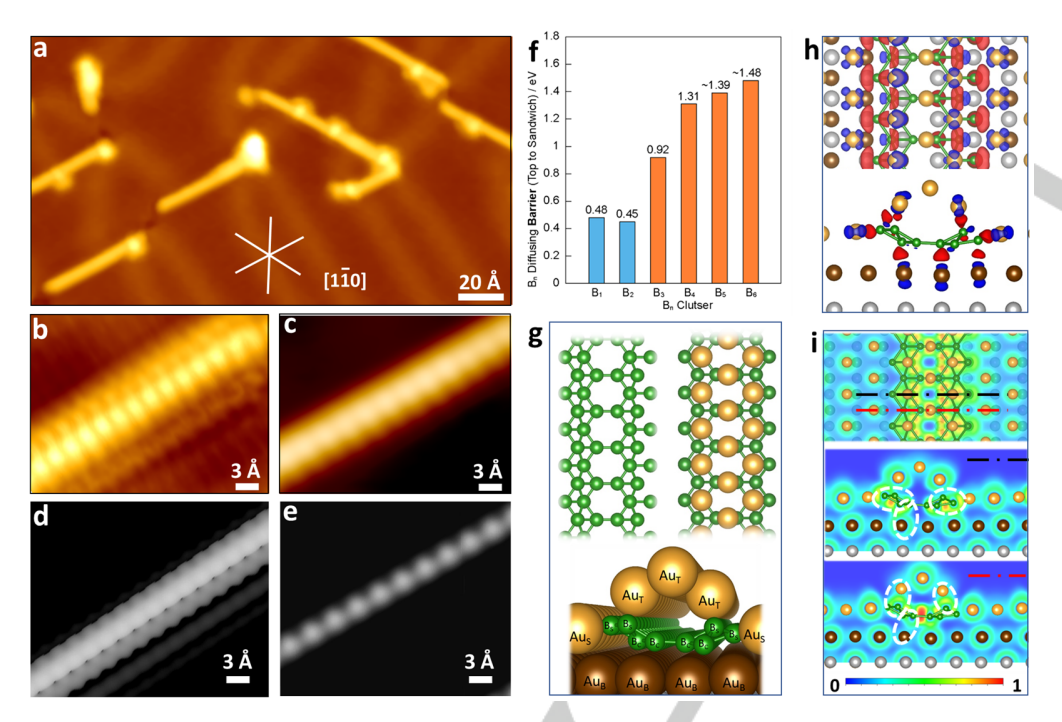


Figure 1. (a) STM image of the 1D BNRs achieved by depositing B atoms on Au(111) kept at RT, where the ribbons are preferentially oriented along the <1-10> directions of the substrate (I = 100 pA, V = +1.0 V). (b–c) Zoom-in STM images of an individual ribbon: when the tip is close to the sample (panel b: I = 5 nA, V = 10 mV), a backbone-like structure with a width of 10.4 Å and a bright central axis are shown; at a large tip-sample distance (panel c: I = 100 pA, V = 1.0 V), a single bright chain is observed. (d) Penetration barrier from the top to the second layer of Au(111) for B units with varying numbers of B atoms (B_n, n = 1-6), showing that the barrier evidently increases with n. (e) Top- and side-view DFT-optimized model for the BNR. B and the top-, second-, and third-layer Au atoms are in green, yellow, brown, and grey, respectively. (f–g) Calculated STM image of a single BNR on Au(111) based on the structural model in panel e, with the applied current and voltage the same as those in panels b and c, respectively, showing a good match with the experimental results. (h) Top and side views of the DFT-calculated electronic density difference plot. The isovalue is 0.05 e/ų. The red and blue colors represent charge accumulation and depletion, respectively. (i) Top and side views of ELF mapping of the BNR on Au(111), where the side views are sliced at the black and red lines, respectively.

By evaporating B atoms at ~2200 K onto Au(111) held at room temperature (RT) for 60-90 s, typical 1D ribbons are formed. The ribbons have a uniform width and lengths up to ~200 Å, essentially along the <1-10> directions of Au(111) (Figure 1a). The ribbons' formation is associated with the dosage and the substrate temperature during B deposition. 1D ribbons are only observed when keeping the substrate at RT and at a B coverage lower than ~0.5 monolayer (ML). The ribbons can coexist with irregular 2D patches. When the coverage is above 0.5 ML, the 2D patches become dominant (Figure S1). The close-view STM image (Figure 1b) reveals that each ribbon appears as a bulging backbone with a width of 10.4 \pm 0.2 Å. A bright chain composed of circular protrusions lies on the central axis, with delicate, dim features regularly aligned on both sides. Both the central chain and the side features both have a periodicity of ~2.9 Å, with the latter shifting relative to the former along the ribbon. At a larger tip-sample distance, the protrusions of the central chain can be observed selectively (Figure 1c).

DFT calculations were used for structural determination. Given that 2D borophene can be fabricated on Au(111)^[26] and freestanding BNRs have been theoretically suggested, [33,34] we initially considered the possibility of forming the ribbons on top of the Au surface. As shown in Figures S2 and S3, BNRs with varying widths (containing three to ten rows of B atoms, where the numbers of B rows are depicted in the side-view models) were calculated on a substrate slab having three layers of Au atoms (details in Supplementary Information, SI). However, in all

cases, the BNRs are unstable and greatly distorted after full relaxation. All the calculated morphology and contrast contradict the experimental findings.

AIMD simulations further ruled out the possibility of forming BNRs on the outermost layer of Au(111) (Figure S4). It is revealed that B single atoms can quickly penetrate the outermost surface of the Au substrate and stabilize between the top two Au layers. DFT calculations show that the most stable site for B monomers (single B atoms) is the subsurface octahedral sites between the top two Au layers. Individual B monomers are not stable on the Au(111) surface. The energy barrier for diffusion to the subsurface is small (0.48 eV), while it is difficult to diffuse deeper. Given the high B evaporation temperature (~2200 K), this penetration barrier is easy to overcome. The penetration is energetically preferred, with an energy gain of 0.41 eV (i.e., 0.41 eV lower than the energy of the initial state) for each monomer. The energy gain is attributed to the increased B-Au interaction when the B atoms travel from the top to the subsurface of Au(111). The size of B clusters has a strong influence on the penetration barrier (Figures 1d and S5). For instance, the barriers for a monomer and a dimer are only 0.48 and 0.45 eV, whilst the barrier for a B trimer increases to 0.92 eV.

This point is supported by the following two-step control experiments. By keeping the substrate at \sim 78 K during B deposition, the penetration dynamics of B atoms are reduced. As anticipated, clusters (with sizes varying from 30 to 50 Å)

develop on the Au surface in the absence of the BNRs (Figure S6). When warming the Au substrate with these B clusters to RT, no BNRs emerge. This is attributed to the high penetration barrier for B clusters. The results confirm that the penetration of B into the substrate is crucial for BNR formation. Consistently, previous work by our group and others^[26,36–38] also demonstrated that small atoms (*e.g.*, B, carbon) can penetrate into Au(111) and Cu(111) and be stabilized at the subsurface.

We then proposed alternate models with the BNRs embedded in the Au outermost layer with the expelled Au atoms on top. To figure out the structural model for the observed 1D ribbon, different cases with various rows of B atoms (three to ten rows) and various rows of expelled Au atoms were calculated. Figures S7 and S8 show the top and side views of the fullyrelaxed model as well as the corresponding calculated STM and STS images for each case. Clearly, the structure with eight rows of B atoms beneath three rows of expelled Au atoms (denoted as '8B-3Au' in Figures 1e and S8b) matches the experimental results. As seen in the top-view model, the BNR has an edge-toedge width of 10.7 Å and a periodicity of 2.9 Å and is composed of a pair of (2,2) zigzag rows, forming hollow hexagons in between. The central-row Au atoms sit on the bridge sites between two B atoms of the hexagons, while each Au atom in the side rows sits near the atop site of a B atom. According to the side-view model (Figures 1e and S9), the BNR has a buckled configuration: the central four B rows are located at nearly the same height (2.2 Å above the subsurface Au layer); the four side B rows (two rows on each side) are lifted up with an increased height: the two rows on one side are of the same height of 3.1 Å, while the rest two rows on the other side are of 2.9 Å and 2.3 Å above the subsurface Au layer, respectively. In keeping with the observed STM results (Figure 1b), the three rows of evacuated Au atoms form a bulging structure. The central and side Au rows are 6.0 and 4.8 Å above the subsurface Au layer, respectively. The B atoms in the four central and four side rows are denoted as 'Bc' and 'Bs', respectively. The morphology, periodicity, width, and tunneling contrast of the calculated STM images (Figures 1f and 1g) based on the 8B-3Au model match the experimental observations (Figures 1b and 1c). The bulging Au row contributes to the central bright chain.

We explored the interaction between the ribbon and the surrounding Au atoms using DFT calculations. In the 8B-3Au model (Figure S9), the four rows of Bc atoms mainly interact with the second layer of Au atoms beneath them (denoted as ' Au_B '), whereas the four rows of Bs atoms interact with the Au atoms on top of the ribbon ('Au τ ') and laterally adjacent to the ribbon sides ('Aus'). The distance between these B atoms and Au atoms is 2.2-2.4 Å. The electron density difference plot (Figure 1h) and electron localization function (ELF) mapping (Figure 1i) demonstrate electron shift from first-layer Au atoms (Aus and Au_T) towards B_S and from second-layer Au atoms (Au_B) towards B_{C} . The preferential interactions drive B_{S} to be higher than B_{C} ; as a result, the BNR adopts a buckled rather than planar configuration. B and Au atoms are weakly coordinated, and the stability of the BNR is primarily attributed to the B-B bonding in the BNR. Thanks to the surrounding Au atoms, the BNR is totally

protected, free of the arduous passivation required for 2D borophenes. [39]

To investigate how the penetrated B atoms diffuse and bond into BNR, we carried out DFT calculations and AIMD simulations at the picosecond scale. It is found that the B monomers migrate easily from one octahedral site to another at the Au subsurface with a minor barrier (0.16 eV) (Figures 2 and S10). When B monomers travel to adjacent octahedral sites, B–B bonds are formed. The evolution from monomers to clusters results in significant energy gain due to these newly formed B–B bonds. Meanwhile, Au atoms in the pristine outermost layer are evacuated. The same accumulating and bonding tendency is observed as the number of subsurface B monomers grows (Figure S11). In this manner, an extended BNR is fabricated.

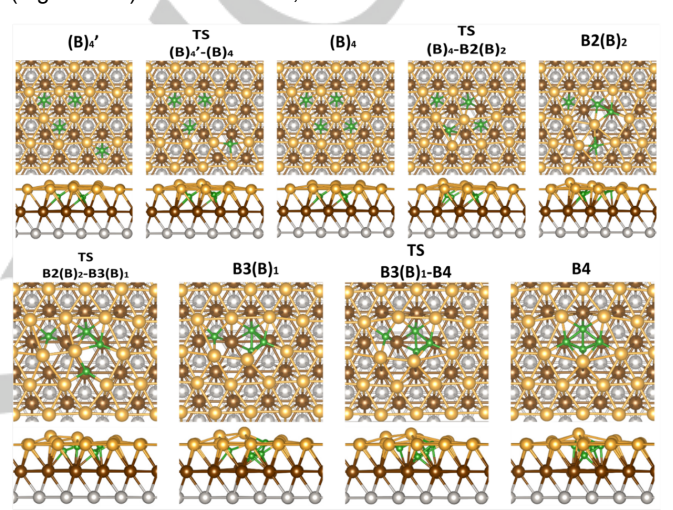


Figure 2. Top- and side-view models of the aggregation and bonding processes of B monomers at the Au subsurface. The four monomers are initially placed at subsurface octahedral sites, with three of them nearby and the fourth distant $[(B)_4]$; the atoms prefer to accumulate together, and the fourth B atom migrates to form the close packing $[(B)_4]$ with the three atoms via the transition state $[TS (B)_4'-(B)_4]$; the individual four monomers gradually evolve through a series of transitions to form a dimer and two monomers $[B2(B)_2]$, then a trimer with one monomer $[B3(B)_1]$, and finally a tetramer $[B_4]$.

To understand why the resulting BNRs cannot be extended into 2D borophenes, we calculated the cohesive energy contribution per B atom and chemical potential (Figure S12) for the various BNR models in Figures S7 and S8. It is found that the growth of ribbon width is self-limiting. The formation is more energetically favored for eight and nine B rows than for other BNR widths. According to Figure 1h, due to the charge shift from Au to B atoms, dipoles form at the BNR's sides, preventing the ribbons from close packing or merging.

To explore the electronic structure of the BNRs, we then acquired *dl/dV* tunneling spectra at the BNR center, the BNR edge, and the Au substrate (marked by the grey, blue, and red crosses in Figure 3a), using a non-functionalized STM tip (Figures 3a–b). In contrast to the Au surface state, both spectra of the BNRs present a shallow asymmetric parabolic curve, with the one from the ribbon edge exhibiting a shoulder in the voltage range of +0.2 to +0.4 V (Figure 3b). The BNR spectra show a typical metallic nature without bandgap, which is consistent with the calculated band structure (Figure S13). We next used STS mapping to further verify the edge state. The spectrum of the Au

surface was recorded before each STS mapping to ascertain that the tip was featureless and consistent. In addition to the diffraction pattern of the electron gas on the Au surface, evident contrast variation from the BNRs is observed when the applied bias voltage is varied from $-1.0~\rm V$ to $+1.0~\rm V$ (Figures 3c–e and S14). At $+0.2~\rm V$ and $+0.4~\rm V$, in particular, a bright outline appears at the edges of each ribbon (Figures 3d and 3e). All these findings indicate that the BNRs have a distinct edge state. Consistently, among the models with various rows of B (three to ten rows) and expelled Au atoms (Figures S7 and S8), only 8B-3Au exhibits the edge state in good agreement with the experimental results (Figure 3e).

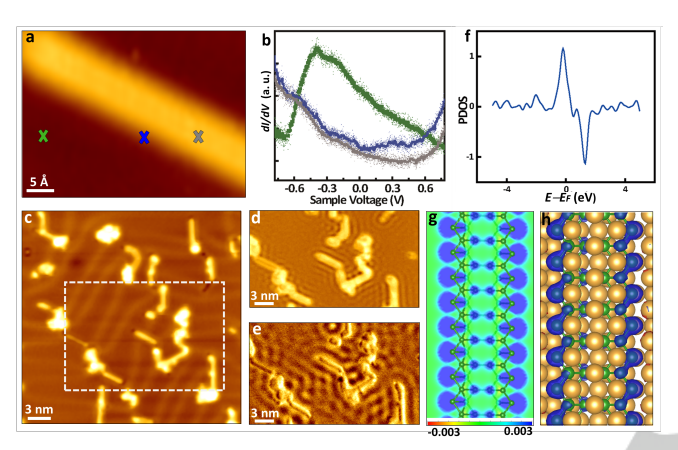


Figure 3. (a) STM image of a BNR. (b) The dl/dV spectra collected from the BNR center (grey), the BNR edge (blue), and the Au surface (green) as marked in panel a. (c) STM image of the BNRs on Au(111) (l=100~pA, V=1.0~V), and (d=0) the corresponding STS mapping at bias voltages of +0.4~V and +0.2~V, respectively (set point of 100 pA), displaying a bright outline at the BNR edges. (f) Calculated PDOS of the net spin density project to the edge B atoms of the freestanding BNR. (g) The net spin density plot sliced at the freestanding BNR (isovalue of $3\times10^{-3}~\text{e-bohr}^{-3}$), showing ferromagnetism with the same- orientation net spin density localized at both edges. (h) Isosurface of the net spin density of the BNR embedded in the Au surface (isovalue of $3\times10^{-6}~\text{e-bohr}^{-3}$).

These edge states are distinct from those of 2D borophenes on Ag(111) which are associated with charge accumulation induced by strong B-Ag bonding.[11] In the present case, the observed edge states cannot be primarily attributed to the B-Au interaction: i) the B atoms are only weakly coordinated with Au atoms; ii) the ribbons are embedded in the top Au layer with expelled Au atoms atop, where the interaction of B atoms with the Au atoms on top and beneath the ribbon is stronger than the edge B atoms with the side Au atoms (Figures 1h and 1i). If the electronic states are attributed to the B-Au interaction, they would not exclusively appear at the ribbon edges. To figure out the possible origin of the edge states, we calculated the spin electron density differential of the BNRs using spin-polarized DFT calculations. For a freestanding ribbon, the density-of-state (DOS) of spin-up states is found to be significantly different from the DOS of spin-down states near Fermi energy (Figure 3f). According to the spin electron density difference plot (Figure 3g), evident spin localization is present at the ribbon edges. Although the unpaired spin is weakened when embedded in Au atoms, the net spin localized at the ribbon edges is still pronounced (Figures 3h and S15). This is further supported by the calculated band structure (Figure S13), which varies between spin-up and

spin-down states, leading to distinct electron state densities for the different spins. As the spins at both ribbon edges are polarized and ferromagnetic-coupled, the ribbons exhibit macroscopic ferromagnetism. The results are in good accordance with the previous theoretical predictions. [21]

In summary, by controlling the growth conditions, supernarrow BNRs consisting of a pair of (2,2) zigzag B rows with a uniform width of 1 nm have been achieved on the Au(111) terrace. The ribbons are formed by spontaneous B atom penetration into the Au substrate, followed by diffusion and bonding at the subsurface. The BNR width is self-confined. The dipoles at the BNRs keep them separated. The BNRs are embedded in the outermost Au layer, with Au atoms shielded on top, free of the arduous post-passivation. Distinct electronic edge states are observed, which is primarily attributed to the spin localization at the BNRs' zigzag edges.

Supporting Information

The authors have included additional references in the Supporting Information. [40-47]

Acknowledgements

This work was financially supported by the National Natural Science Foundation of China (22272041, 22033005, 22022504), the US National Science Foundation (CHE-2403841 to L.S.W.), and Guangdong Provincial Key Laboratory of Catalysis (No. 2020B121201002). Computational resources were supported by Taiyi high-performance supercomputer cluster of Center for Computational Science and Engineering of Southern University of Science and Technology, and high-performace supercomputer cluster of department of chemistry (CHEM-HPC) of Southern University of Science and Technology.

Conflict of interest

The authors declare no conflict of interest.

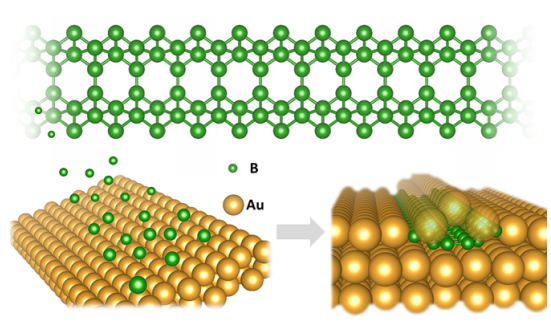
Keywords: borophene • nanoribbon • edge state • formation mechanism • scanning tunneling microscopy

- [1] W. G. Woods, Environ. Health Perspect. 1994, 102, 5–11.
- [2] T. Ogitsu, E. Schwegler, G. Galli, Chem. Rev. 2013, 113, 3425-3449.
- [3] A. P. Sergeeva, I. A. Popov, Z. A. Piazza, W. L. Li, C. Romanescu, L. S. Wang, A. I. Boldyrev, Acc. Chem. Res. 2014, 47, 1349–1358.
- [4] Z. Q. Wang, T. Y. Lu, H. Q. Wang, Y. P. Feng, Front. Phys. 2019, 14, 33403.
- [5] L. S. Wang, Int. Rev. Phys. Chem. 2016, 35, 69-142.
- [6] T. Jian, X. Chen, S. D. Li, A. I. Boldyrev, J. Li, L. S. Wang, Chem. Soc. Rev. 2019, 48, 3550–3591.
- [7] H. J. Zhai, Y. F. Zhao, W. L. Li, Q. Chen, H. Bai, H. S. Hu, Z. A. Piazza, W. J. Tian, H. G. Lu, Y. B. Wu, Y. W. Mu, G. F. Wei, Z. P. Liu, J. Li, S. D. Li, L. S. Wang, Nat. Chem. 2014, 6, 727–731.
- [8] Z. A. Piazza, H. S. Hu, W. L. Li, Y. F. Zhao, J. Li, L. S. Wang, *Nat. Comm.* 2014, 5, 3113.
- [9] W. L. Li, X. Chen, T. Jian, T. T. Chen, J. Li, L. S. Wang, *Nat. Rev. Chem.* 2017, 1, 9.

[10] A. J. Mannix, X. F. Zhou, B. Kiraly, J. D. Wood, D. Alducin, B. D. Myers, X. Liu, B. L. Fisher, U. Santiago, J. R. Guest, M. J. Yacaman, A. Ponce, A. R. Oganov, M. C. Hersam, N. P. Guisinger, Science 2015, 350, 1513–1516.

- [11] B. Feng, J. Zhang, Q. Zhong, W. Li, S. Li, H. Li, P. Cheng, S. Meng, L. Chen, K. Wu, *Nat. Chem.* **2016**, *8*, 564–569.
- [12] H. Tang, S. Ismail-Beigi, Phys. Rev. Lett. 2007, 99, 115501.
- [13] X. Liu, Z. Zhang, L. Wang, B. I. Yakobson, Nat. Mater. 2018, 17, 783–787.
- [14] L. Kong, L. Liu, L. Chen, Q. Zhong, P. Cheng, H. Li, Z. Zhang, K. Wu, Nanoscale 2019, 11, 15605–15611.
- [15] Y. Wang, L. Kong, C. Chen, P. Cheng, B. Feng, K. Wu, L. Chen, Adv. Mater. 2020, 32, 2005128.
- [16] B. Feng, O. Sugino, R. Y. Liu, J. Zhang, R. Yukawa, M. Kawamura, T. limori, H. Kim, Y. Hasegawa, H. Li, L. Chen, K. Wu, H. Kumigashira, F. Komori, T.C. Chiang, S. Meng, I. Matsuda, *Phys. Rev. Lett.* 2017, 118, 096401.
- [17] B. Feng, J. Zhang, S. Ito, M. Arita, C. Cheng, L. Chen, K. Wu, F. Komori, O. Sugin, K. Miyamoto, T. Okuda, S. Meng, I. Matsuda, *Adv. Mater.* 2018, 30, 1704025.
- [18] E. S. Penev, A. Kutana, B. I. Yakobson, Nano Lett. 2016, 16, 2522-2526.
- [19] Z. Zhang, A. J. Mannix, Z. Hu, B. Kiraly, N. P. Guisinger, M. C. Hersam, B. I. Yakobson, *Nano Lett.* **2016**, *16*, 6622–6627.
- [20] Z. Zhang, Y. Yang, E. S. Penev, B. I. Yakobson, Adv. Funct. Mater. 2017, 27, 1605059.
- [21] E. S. Penev, S. Bhowmick, A. Sadrzadeh, B. I. Yakobson, *Nano Lett.* 2012, 12, 2441–2445.
- [22] R. Wu, S. Eltinge, I. K. Drozdov, A. Gozar, P. Zahl, J. T. Sadowski, S. Ismail-Beigi, I. Bozovic, Nat. Chem. 2022, 14, 377.
- [23] X. Liu, Q. Li, Q. Ruan, M. S. Rahn, B. I. Yakobson, M. C. Hersam, *Nat. Mater.* 2022, 21, 35–40.
- [24] C. Chen, H. Lv, P. Zhang, Z. Zhuo, Y. Wang, C. Ma, W. Li, X. Wang, B. Feng, P. Cheng, X. Wu, K. Wu, L. Chen, Nat. Chem. 2022, 14, 25–31.
- [25] R. Wu, I. K. Drozdov, S. Eltinge, P. Zahl, S. Ismail-Beigi, I. Bozovic, A. Gozar, Nat. Nanotech. 2019, 14, 44–49.
- [26] B. Kiraly, X. Liu, L. Wang, Z. Zhang, A. J. Mannix, B. L. Fisher, B. I. Yakobson, M. C. Hersam, N. P. Guisinger, ACS Nano 2019, 13, 2816, 3822
- [27] Q. Zhong, L. Kong, J. Gou, W. Li, S. Sheng, S. Yang, P. Cheng, H. Li, K. Wu, L. Chen, *Phys. Rev. Mater.* 2017, 1, 021001(R).

- [28] L. Talirz, P. Ruffieux, R. Fasel, Adv. Mater. 2016, 28, 6222-6231.
- [29] P. Ruffieux, S. Wang, B. Yang, C. Sanchez-Sanchez, J. Liu, T. Dienel, L. Talirz, P. Shinde, C. A. Pignedoli, D. Passerone, T. Dumslaff, X. Feng, K. Muellen, R. Fasel, *Nature* 2016, 531, 489–493.
- [30] J. M. Cai, P. Ruffieux, R. Jaafar, M. Bieri, T. Braun, S. Blankenburg, M. Muoth, A. P. Seitsonen, M. Saleh, X. L. Feng, K. Mullen, R. Fasel, *Nature* 2010, 466, 470–473.
- [31] T. Cao, F. Z. Zhao, S. G. Louie, Phys. Rev. Lett. 2017, 119, 076401.
- [32] D. J. Rizzo, G. Veber, T. Cao, C. Bronner, T. Chen, F. Zhao, H. Rodriguez, S. G. Louie, M. F. Crommie, F. R. Fischer, *Nature* 2018, 560, 204–208.
- [33] S. I. Vishkayi, M. B. Tagani, Nano-Micro Lett. 2018, 10, 14.
- [34] S. Saxena, T. A. Tyson, Phys. Rev. Lett. 2010, 104, 245502.
- [35] Q. Li, L. Wang, H. Li, M. K. Y. Chan, M. C. Hersam, ACS Nano 2024, 18, 483–491
- [36] R. Wu, A. Gozar, I. Bozovic, NPJ Quantum Mater. 2019, 4, 40.
- [37] S. Wang, P. Ding, Z. Li, C. Mattioli, W. E, Y. Sun, A. Gourdon, L. N. Kantorovich, F. Besenbacher, X. Yang, M. Yu, Angew. Chem. Int. Ed. 2021, 60, 23123–23127.
- [38] Y. Zhou, F. Che, M. Liu, C. Zou, Z. Liang, P. De Luna, H. Yuan, J. Li, Z. Wang, H. Xie, H. Li, P. Chen, E. Bladt, R. Quintero-Bermudez, T. K. Sham, S. Bals, J. Hofkens, D. Sinton, G. Chen, E. H. Sargent, *Nat. Chem.* 2018, 10, 974–980.
- [39] Q. Li, V. S. C. Kolluru, M. S. Rahn, E. Schwenker, S. Li, R. G. Hennig, P. Darancet, M. K. Y. Chan, M. C. Hersam, *Science* 2021, 371, 1143–1148.
- [40] G. Kresse, J. Furthmuller, *Phys. Rev. B* **1996**, *54*, 11169–11186.
- [41] G. Kresse, D. Joubert, Phys. Rev. B 1999, 59, 1758-1775.
- [42] J. P. Perdew, K. Burke, M. Ernzerhof, Phys. Rev. Lett. 1997, 77, 3865–3868.
- [43] S. Grimme, J. Antony, S. Ehrlich, H. Krieg, J. Chem. Phys. 2010, 132, 154104.
- [44] G. Henkelman, H. Jonsson, J. Chem. Phys. 2000, 113, 9978-9985.
- [45] S. Nose, J. Chem. Phys. 1984, 81, 511-519.
- [46] W. G. Hoover, Phys. Rev. A 1985, 31, 1695-1697.
- [47] N. Friedrich, P. Brandimarte, J. Li, S. Saito, S. Yamaguchi, I. Pozo, D. Pena, T. Frederiksen, A. Garcia-Lekue, D. Sanchez-Portal, J. Ignacio Pascual, *Phys. Rev. Lett.* 2020, 125, 146801.



The formation of supernarrow borophene nanoribbons has been experimentally realized. The ribbons have a uniform width of \sim 10 Å and can be as long as 200 Å. They are embedded in the outermost layer of Au(111) and shielded on top by evacuated Au atoms. Distinct edge states are revealed from the ribbons, which are primarily attributed to the localized spin at their zigzag edges.

